Mexican Journal of Phytopathology
e-ISSN: 2007-8080

Crossref
Open access

Phytopathological Note

Spatial behavior of iron spot (*Mycosphaerella coffeicola*) in coffee plantations in Amatepec, State of Mexico

José Francisco Ramírez-Dávila[1], Fidel Lara-Vázquez[1]*, Dulce Karen Figueroa-Figueroa[1], María Teresa Lugo-Coyote[1]. [1]Facultad de Ciencias Agrícolas de la Universidad Autónoma del Estado de México. Campus El Cerrillo, Carretera Toluca-Ixtlahuaca Km 15.5, Piedras Blancas, 50200 Toluca de Lerdo, México.

Corresponding Author:
Fidel Lara-Vázquez
fidel.lara@hotmail.com

Section:
Periodical Issue

Reviewed:
March 14, 2025
Published:
December 20, 2025
Early Access 2026

Citation:
Ramírez-Dávila JF, Lara-Vázquez F, Figueroa-Figueroa DK and Lugo-Coyote MT. 2026. Spatial behavior of iron spot (*Mycosphaerella coffeicola*) in coffee plantations in Amatepec, State of Mexico. Mexican Journal of Phytopathology 44(1): 106. https://doi.org/10.18781/R.MEX.FIT.2212-5.

ABSTRACT

Background/Objective. Coffee production in the State of Mexico, particularly in the municipality of Amatepec, is threatened by several diseases, including iron spot caused by *Mycosphaerella coffeicola*. This foliar disease negatively affects coffee yield and quality. The objective of this study was to model the spatial distribution of iron spot in coffee plantations in Amatepec using classical statistics and geostatistics, estimating the infected area to economically evaluate management strategies.

Experimental development. In six coffee plots planted with the cultivars Caturra and Typica, 100 plants per plot were georeferenced using a quadrant sampling method and monitored biweekly for six months. From each plant, 36 leaves were sampled considering the four cardinal points and three canopy strata (upper, middle, and lower). Data were analyzed using classical statistics (dispersion and Green's indices, Poisson and Negative Binomial distributions) and geostatistics (theoretical semivariograms and Ordinary Kriging).

Results. Classical statistics indicated an aggregated distribution of the disease but lacked sufficient spatial precision. Geostatistical analysis generated theoretical semivariograms (Gaussian, Spherical, and Exponential models) and Ordinary Kriging maps that clearly visualized disease distribution. This approach allowed the identification of infection foci and a reliable estimation of the infected area, supporting precision management strategies.

Conclusion. Geostatistics provided greater precision than classical statistics for spatial analysis of iron spot. Ordinary Kriging maps identified areas with and without disease presence, enabling more efficient and targeted management actions.

Keywords: Geostatistics, Interpolation, Ordinary Kriging, Spatial variability

INTRODUCTION

Coffee cultivation is considered a strategic activity in Mexico. Mexico is currently the ninth-largest producer, with a production volume of 1 056 305.93 t of "green" coffee beans. Of all Mexican coffee exports, 53.8% are destined for the United States; the remaining volume goes to member countries of the European Union and to others such as Japan, Cuba, and Canada (SIAP, 2025).

It is noteworthy that in recent years the recognition of coffee from the State of Mexico has increased, as two growers from the region have achieved outstanding results in the "Cup of Excellence," earning scores above 90.0 points (Leguizamo *et al.*, 2023). However, one of the main challenges faced by coffee producers is the occurrence of phytopathologies during each production cycle at the regional, national, and even international levels. Among the most important diseases affecting coffee cultivation is iron spot, caused by a facultative parasitic fungus that exhibits two reproductive stages in its life cycle: the teleomorph, caused by *Mycosphaerella coffeicola*, and the anamorph, caused by *Cercospora coffeicola* (Guzmán and Rivillas, 2008). *Cercospora coffeicola* severely affects coffee quality by inducing leaf drop and promoting premature ripening and abscission of fruits, leading to yield losses of up to 30% (Ramos *et al.*, 2021).

The spatial distribution of individuals within a population dispersed over a given area has been studied using statistical distributions and dispersion indices, with an emphasis on the precise spatial location of individuals. This approach overcomes limitations inherent to traditional methods and opens new avenues for research and resource management (Acosta-Guadarrama *et al.*, 2017). Geostatistical methods provide the distribution of organisms based on their exact spatial location and generate highly useful maps (Rossi *et al.*, 1992), allowing the identification of spatial distribution patterns. Such maps make it possible to determine infection levels requiring immediate control, to detect potential preferences in aggregation structure, and to identify areas with no infection (Acosta-Guadarrama *et al.*, 2017; Rivera *et al.*, 2018).

Therefore, the objective of this study was to model, using classical statistics and geostatistics, the spatial distribution of the fungus *Mycosphaerella coffeicola*, the causal agent of iron spot, in order to estimate the affected area and conduct an economic evaluation in coffee plantations in the municipality of Amatepec, State of Mexico.

EXPERIMENTAL DEVELOPMENT

Study area. The study was conducted in the coffee-producing area of the municipality of Amatepec, State of Mexico, where six commercial coffee plots were selected. These plots followed a traditional polyculture system with conventionally managed Caturra and Typica coffee varieties, under 40–60% shade composed of parota (*Enterolobium cyclocarpum*), ash (*Fraxinus* spp.), orange (*Citrus sinensis*), lemon (*Citrus limon*), and semi-woody species such as castor bean (*Ricinus communis*). The plantations were less than 10 years old. The soil type was classified as sandy-loam regosols with a depth of 30 cm. Four plots had moderate slopes of 8–15%, while the remaining two had steep slopes of 15–30%. Each plot consisted of half a hectare, divided into 10 × 10 m quadrants, for a total of 50 quadrants per plot. Using the quadrant sampling method, two plants per quadrant were selected at random, totaling 100 plants in each plot (Maldonado *et al.*, 2017; Rivera *et al.*, 2018). Each plant was georeferenced with a differential global positioning system (DGPS, Trimble

SPS361 model) and marked for data collection (Rivera *et al.*, 2018; Pino-Miranda *et al.*, 2022).

Biweekly sampling was conducted in the six plots over six months (September 2021 to February 2022), covering different phenological stages (September: "milky fruit"; October–December: "firm fruit"; January–February: "ripe fruit"). A total of 36 leaves per plant were examined, recording three symptomatic leaves per branch; each branch was selected from the four cardinal points, dividing the plant into upper, middle, and lower strata. The presence of iron spot was determined based on the absence or presence of symptoms on the sampled leaves (Tapia-Rodríguez *et al.*, 2020).

To distinguish the symptoms of the disease under study from those of other diseases such as American leaf spot (*Mycena citricolor*) and coffee rust (*Hemileia vastatrix*), characteristics such as brown lesions with a chlorotic or yellowish halo contrasting with the healthy leaf tissue were considered; as the disease progresses, these lesions increase in size and lead to tissue necrosis (SENASICA, 2016). In addition, leaves showing signs of the fungus were collected and transported to the Laboratory of Entomological and Technological Research in Precision Agriculture of the Facultad de Ciencias Agrícolas, UAEMex, State of Mexico, for the identification of *Mycosphaerella coffeicola* (sexual state, teleomorph). The fungus was isolated on Coffee Oat Agar medium, and morphological characterization was performed by microscopy following the descriptive information provided by the Servicio Nacional de Sanidad, Inocuidad y Calidad Agroalimentaria (SENASICA, 2016).

Classical statistics. The spatial distribution of the organisms observed in this study was established using two general methods (Negative Binomial and Poisson), as well as by calculating dispersion indices (Dispersion and Green's indices). Both approaches were applied to enable a pertinent comparison between the results obtained from non-spatial statistics and spatial statistics. For all statistical distributions, the MLP maximum-likelihood program was used to fit the models to the outlined data. Model fit was evaluated using a test2 (Ramírez and Sánchez, 2011).

Geostatistical analysis. Experimental semivariograms from each sampling event were estimated and fitted to predefined models in the software Variowin 2.2 (Software for Spatial Data Analysis in 2D, New York, USA). Once the semivariograms were estimated and modeled, the error incurred when assigning the average value of a series of point measurements to a larger domain was determined and calculated using the following formula (Isaaks and Srivastava, 1988; Pino-Miranda *et al.*, 2022):

$$\gamma^{*}(\mathrm{h}) = \frac{1}{2\mathrm{N}(\mathrm{h})}\sum_{i=1}^{\mathrm{N}(\mathrm{h})}[z(x_i+\mathrm{h})-\mathrm{z}(x_i)]^2$$

Where: γ^* is the experimental semivariogram value for the distance interval h; $n(h)$ is the number of pairs of sampling points separated by the distance interval h; $z(x_i)$ is the value of the variable of interest at sampling point x_i; and $z(x_i + h)$ is the value of the variable of interest at sampling point $x_i + h$.

The experimental semivariograms were fitted to different theoretical models. During model validation, an iterative process was carried out to achieve the best possible fit and to ensure the model's accuracy and effectiveness. The evaluated model parameters included the nugget effect (Co), the sill (C), and the range (a). Once the experimental semivariograms were fitted to the theoretical models, they were statistically validated using parameters such as the Mean Estimation Error (MEE), Mean Squared Error (MSE), and Dimensionless Mean Squared Error (DMSE) (Maldonado *et al.*, 2017; Acosta-Guadarrama *et al.*, 2017; Tapia-Rodríguez *et al.*, 2020).

Spatial dependence level. The evaluation of spatial dependence allowed the establishment of a significant relationship among the sampling data. Values were obtained by dividing the nugget effect by the sill and expressing the result as a percentage. If the result is less than 25%, the level of spatial dependence is considered high; if it is between 26% and 75%, the level is moderate; and if it exceeds 76%, it is considered low (Maldonado *et al.*, 2017).

Map construction. Maps were generated by interpolating the absence and presence of the disease using Ordinary Kriging, which allows for unbiased estimation of values at unsampled points because the sample mean and variance are known (Díaz *et al.*, 2018). The infected area was determined, and the maps were produced using Surfer 16.0 "Surface Mapping System, Golden Software" (Rivera *et al.*, 2018).

Estimation of infected plant area and its economic impact. To estimate the area with plants infected by *Mycosphaerella coffeicola* and assess its economic impact, maps were generated using Ordinary Kriging in the Surfer 16.0 program. Based on the percentage of infected area in each map, the cost of a full-plot fungicide application of Controller F-500 (flutriafol) was calculated, as well as the cost of a targeted application (infected areas only). The difference between these costs represents the potential economic savings of the precision methodology. Similarly, the amount of phytosanitary product required under both strategies was quantified. In this way, a possible reduction in environmental impact is inferred, as the decrease in fungicide use for managing this disease suggests lower pressure on the ecosystem (Ramírez-Dávila and Porcayo-Camargo, 2008).

Classical statistics. According to the type of spatial distribution of iron spot obtained in each sampling event, the results are presented in Table 1. The dispersion index indicates that in most samplings the disease exhibited an aggregated distribution; however, random distributions were also observed. These occurred in Plot 1 during samplings six, nine, and eleven; in Plot 3 during samplings three, eight, and eleven; in Plot 4 during samplings nine and eleven; and in Plot 6 during samplings seven and nine.

With respect to Green's index, this aggregation is confirmed (Table 1). Among the conducted samplings, some aggregated patterns showed low positive values of Green's index, indicating a weak level of aggregation. However, there were also samplings with values of Green's index close to zero, suggesting a random distribution of the disease: in Plot 1 during samplings two, four, and nine; in Plot 3 during samplings five and nine; in Plot 5 during samplings two, six, and nine; and in Plot 6 during samplings two and ten (Ramírez and Sánchez, 2011). The analysis shows that the method is effective for detecting disease aggregation, but it also highlights the need to improve precision in determining the spatial distribution.

Likewise, based on the statistical distributions (Table 1), the results indicate that in Plot 1 during all samplings except samplings three and seven; in Plot 4 during samplings two, three, four, five, six, seven, eight, nine, eleven, and twelve; and in Plot 6 during samplings two, three, four, six, seven, eight, ten, eleven, and twelve, the data fitted a Negative Binomial distribution (aggregation).

Conversely, Table 1 shows that in Plot 1 during sampling six; in Plot 3 during samplings two and ten; and in Plot 5 during samplings two and five, the data fitted a Poisson distribution (random). In these cases, it is not possible to discern a true spatial distribution of iron spot in the monitored plots, as the disease cannot simultaneously exhibit two different spatial distributions.

The apparent duality observed in the results—where the data can fit both the Poisson and Negative Binomial distributions—suggests a valuable opportunity to deepen our understanding of the factors influencing the spatial distribution of organisms. The tendency of the Negative Binomial distribution to converge toward the Poisson distribution when the parameter k is high invites further exploration of the conditions under which this transition occurs.

The discrepancies observed between the dispersion index and Green's index—for example, in Plot 1 during sampling six, where the dispersion index indicates randomness while Green's index indicates aggregation—should not be interpreted as contradictions. Instead, they represent an opportunity to refine these analytical methodologies. These results highlight the importance of considering multiple approaches when interpreting outcomes within the specific context of the study.

Finally, the difficulty in adjusting parameter k in certain samplings—Plot 1 in samplings three and seven; Plot 3 in sampling eleven; Plot 4 in samplings one and ten; and Plot 6 in samplings one, five, and nine—due to the inability to achieve correlation in the maximum-likelihood adjustment logs, provides a basis for advancing our understanding of the complexities inherent in non-spatial statistics. Rather than representing a simple limitation, these results underscore the importance of exploring and developing complementary or alternative methodologies. They invite further investigation into the possible causes of this lack of fit, whether due to data characteristics or the need to refine the statistical models used, as well as promoting a deeper understanding of the crop and the main pathogens under study.

Geostatistical analysis. The Ordinary Kriging technique was used for the spatial interpolation of iron spot incidence, resulting in detailed maps of its distribution. Unlike other methods, Kriging allowed the spatial continuity of the disease (spatial pattern) to be described and its variation across space to be quantified. This capability is crucial, as it enables the prediction of incidence at unsampled locations based on distance and the degree of spatial relationship with measured data, facilitating the identification of risk zones. The generated maps show the different aggregation points of iron spot in the various plots studied (Figure 1). It should be noted that these maps visually reveal how the spatial behavior of the disease evolves over time.

The maps obtained for the area exhibiting iron spot in Plot 1 show that in September and October the aggregation centers or infection foci were located along the western (left) and eastern (right) edges, with a tendency toward the center of the plot. Regarding the phenological stage in September, the fruits were in the milky stage, with an average temperature of 25.8 °C and a relative humidity of 85%. In October, the fruits began the month in the milky stage, with a temperature of 24.3 °C and a relative humidity of 73%.

Table 1. Dispersion indices and statistical distribution of iron spot (*Mycosphaerella coffeicola*) in coffee plots in the municipality of Amatepec, State of Mexico. Sampling conducted from September 2021 to February 2022.

Plot 1	Dispersion index	Green's index	Poisson distribution	Negative Binomial distribution	*k*
1) Sep-01	1.68s	0.21	NS	S	2.68
2) Sep-02	2.08s	0.00	NS	S	3.17
3) Oct-03	1.33s	0.69	NA	NA	-
4) Oct-04	1.47s	0.00	NS	S	5.22
5) Nov-05	2.52s	0.75	NS	S	1.05
6) Nov-06	0.77ns	0.25	S	S	25.02
7) Dic-07	2.88s	0.92	NA	NA	-
8) Dic-08	2.67s	0.73	NS	S	8.41
9) Ene-09	0.51ns	0.00	NS	S	6.11
10) Ene-10	1.37s	0.44	NS	S	7.19
11) Feb-11	0.24ns	0.15	NS	S	2.96
12) Feb-12	3.12s	0.94	NS	S	8.26

Plot 2	Dispersion index	Green's index	Poisson distribution	Negative Binomial distribution	*k*
1) Sep-01	1.77s	0.00	NS	S	0.57
2) Sep-02	2.48s	0.24	NS	S	1.72
3) Oct-03	1.61s	0.92	NS	S	10.04
4) Oct-04	2.88s	0.73	NA	NA	-
5) Nov-05	0.54ns	0.17	NS	S	4.23
6) Nov-06	3.07s	0.49	NS	S	2.08
7) Dic-07	2.67s	0.11	NS	S	8.22
8) Dic-08	0.33ns	0.98	NS	S	7.19
9) Ene-09	2.25s	0.00	NS	S	4.74
10) Ene-10	1.57s	0.57	NA	NA	2.73
11) Feb-11	3.07s	0.49	NS	S	2.08
12) Feb-12	2.48s	0.24	NS	S	1.72

Plot 3	Dispersion index	Green's index	Poisson distribution	Negative Binomial distribution	*k*
1) Sep-01	2.63s	0.55	NS	S	4.25
2) Sep-02	1.09s	0.42	S	S	29.69
3) Oct-03	0.27ns	0.87	NS	S	10.66
4) Oct-04	3.29s	0.27	NS	S	7.36
5) Nov-05	2.44s	0.00	NS	S	2.08
6) Nov-06	1.53s	0.63	NS	S	1.54
7) Dic-07	2.78s	0.72	NS	S	5.71
8) Dic-08	0.66ns	0.16	NS	S	6.42
9) Ene-09	1.40s	0.00	NS	S	9.11
10) Ene-10	1.38s	0.95	S	S	36.15
11) Feb-11	0.52ns	0.50	NA	NA	-
12) Feb-12	1.57s	0.12	NS	S	6.01

Plot 4	Dispersion index	Green's index	Poisson distribution	Negative Binomial distribution	*k*
1) Sep-01	1.24s	0.65	NA	NA	-
2) Sep-02	1.92s	0.24	NS	S	4.67
3) Oct-03	1.57s	0.00	NS	S	1.83
4) Oct-04	2.44s	0.00	NS	S	9.25
5) Nov-05	1.73s	0.58	NS	S	5.66
6) Nov-06	3.22s	0.33	NS	S	2.89
7) Dic-07	2.94s	0.81	NS	S	1.92
8) Dic-08	1.77s	0.00	NS	S	0.48
9) Ene-09	0.70ns	0.95	NS	S	5.27
10) Ene-10	1.24s	0.44	NA	NA	-
11) Feb-11	0.54ns	0.59	NS	S	7.33
12) Feb-12	2.85s	0.37	NS	S	2.21

Plot 5	Dispersion index	Green's index	Poisson distribution	Negative Binomial distribution	*k*
1) Sep-01	3.56	0.55	NS	S	0.93
2) Sep-02	2.47	0.00	S	S	27.14
3) Oct-03	1.73	0.41	NS	S	5.27
4) Oct-04	1.89	0.95	NS	S	1.42
5) Nov-05	0.43ns	0.36	S	S	33.61
6) Nov-06	3.11	0.00	NS	S	8.49
7) Dic-07	2.53	0.22	NS	S	5.27
8) Dic-08	2.82	0.8	NS	S	1.94
9) Ene-09	1.34	0.00	NA	NA	-
10) Ene-10	0.81ns	0.11	NS	S	0.58
11) Feb-11	1.07	0.32	NS	S	9.22
12) Feb-12	0.56ns	0.66	NS	S	4.05

Plot 6	Dispersion index	Green's index	Poisson distribution	Negative Binomial distribution	*k*
1) Sep-01	2.26s	0.56	NA	NA	-
2) Sep-02	3.07s	0.00	NS	S	5.52
3) Oct-03	3.45s	0.78	NS	S	8.13
4) Oct-04	2.87s	0.31	NS	S	0.68
5) Nov-05	1.44s	0.58	NA	NA	-
6) Nov-06	2.02s	0.26	NS	S	1.45
7) Dic-07	0.46ns	0.77	NS	S	7.06
8) Dic-08	2.65s	0.14	NS	S	3.27
9) Ene-09	0.22ns	0.84	NA	NA	-
10) Ene-10	1.24s	0.00	NS	S	1.78
11) Feb-11	2.21s	0.37	NS	S	0.42
12) Feb-12	1.75s	0.99	NS	S	8.13

n): plot number; S: significant; NS: not significant; significance level at 5%. NA: does not fit

In November and December, the aggregation centers were located in the central part of the western (left) side, with a trend toward the northern (upper) portion of the plot. During this period, the fruits were in the firm stage. In November, the average temperature was 19.5 °C with a relative humidity of 65%, while in December the temperature was 18.02 °C and the relative humidity 56%.

In January and February, the infection foci shifted to the northwestern (upper-left) area of the plot. In both months, the fruits were in the ripe stage, with average temperatures of 18.5 and 21.6 °C and relative humidities of 53% and 44% for January and February, respectively (Figure 1).

The semivariograms for Plots 1 and 2 were fully fitted to the spherical model from September through February. In Plot 3, the semivariograms from September to the first half of December fitted the Gaussian model, while those from the second half of December fitted the spherical model. In the first half of January, the semivariogram fitted the Gaussian model, whereas in the second half of January it fitted the spherical model. In the first half of February, the plot again fitted the Gaussian model, and in the second half of February it fitted the exponential model (Table 2).

The nugget effect value was zero in all plots. This value indicates that the sampling used in the present study was adequate and that sampling error was minimal. It suggests that the distance between sampling points was sufficient to capture most of the spatial variability relevant to the study (Table 2). All models showed a high level of spatial dependence for each plot (Table 2). The range values varied from a minimum of 6 m to a maximum of 15 m across the different plots, representing the maximum distance at which spatial correlation among the data exists.

Table 3 shows the results for the percentage of infected area. Plot 6 had the highest infected area (75%) during the second half of November, while the lowest percentage of infection was recorded in Plot 4 during the second half of February (38%). This may be due to specific environmental factors within the plots (microclimate, soil type, management, etc.) that limit disease severity even when the pathogen is present.

Estimation of infected plant area and its economic impact. Producers apply on average 0.5 L ha^{-1} of the systemic fungicide Controller F-500, at a cost of $1,300 pesos per liter (September 2021). A full-coverage application of this product over one hectare would therefore cost $650 pesos. In practical terms, the economic savings ranged from $176 in Plot 6 to $345 in Plot 5 (Table 4). Selective application, in contrast to the traditional uniform method, could generate economic benefits, given that this fungicide is routinely applied in the study area.

Classical statistics. Pérez *et al.* (2023), in their study on the behavior of coffee rust (*Hemileia vastatrix*) populations, used both classical and spatial statistics (geostatistics). Their results emphasized that classical statistics has limitations for determining the physical location of the pathogen. In contrast, spatial statistics can generate maps of the spatial distribution of populations. Similarly, Schotzko and O'Keeffe (1989) provide evidence of how geostatistics in agroecosystems reveals aggregation patterns that offer a more detailed understanding than classical methods, which may overlook or incorrectly describe such patterns.

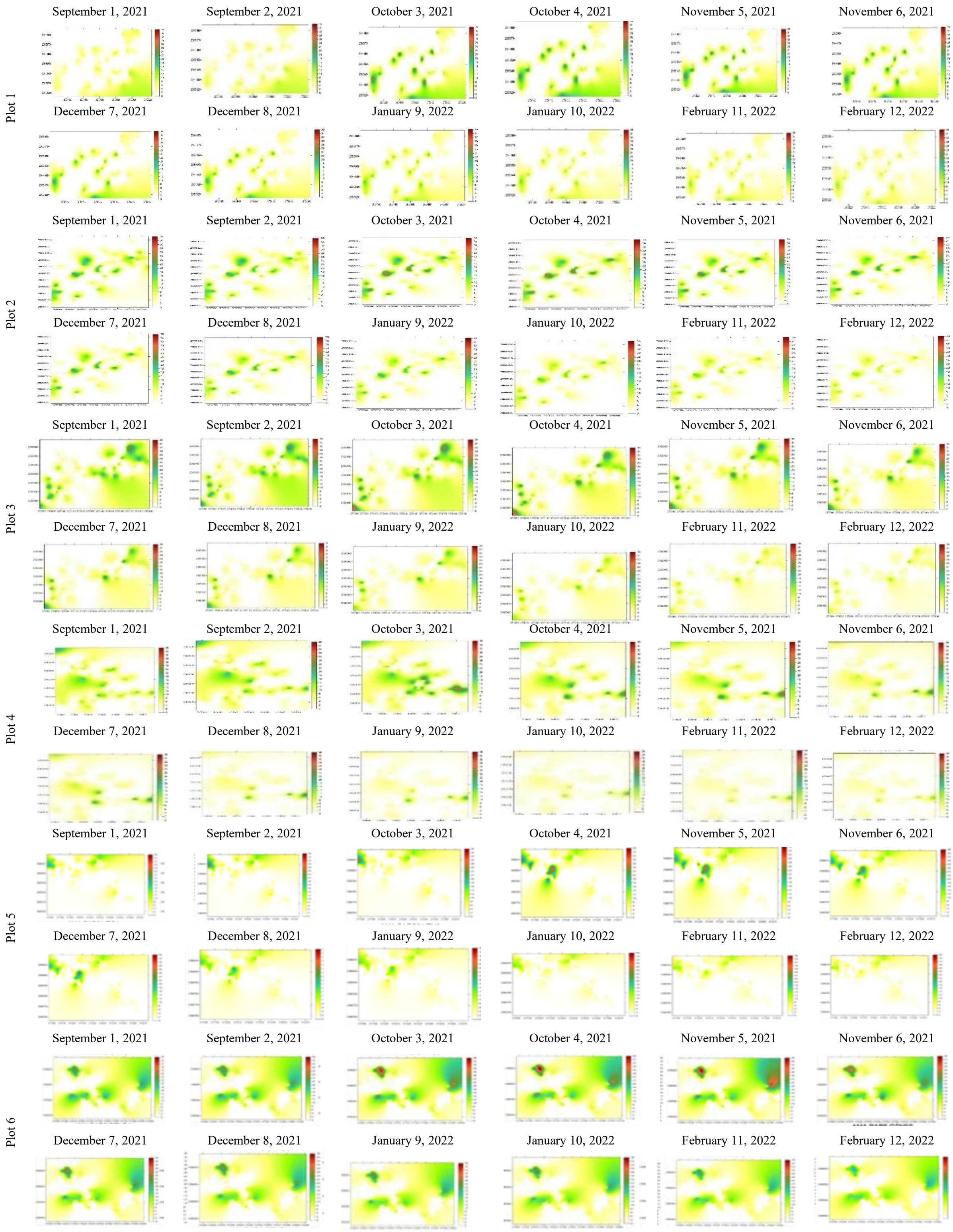

Figure 1. Spatial distribution of the proportion of sampling units with iron spot symptoms in coffee plots in the municipality of Amatepec, State of Mexico, during samplings from September 2021 to February 2022.

Table 2. Parameters (nugget effect, sill, and range) of models fitted to the semivariograms of *Mycosphaerella coffeicola* in coffee plots in the municipality of Amatepec, State of Mexico, from September 2021 to February 2022.

Plot 1	Mean	Variance	Model	Nugget	Sill	Range	Nugget/Sill	Spatial dependence
1) Sep-01	3.43	39.28	Esférico	0	77.44	12.6	0	Alta
2) Sep-02	3.21	35.77	Esférico	0	75.53	11.99	0	Alta
3) Oct-03	3.03	33.62	Esférico	0	71.34	12.60	0	Alta
4) Oct-04	3.17	35.66	Esférico	0	69.66	12.59	0	Alta
5) Nov-05	3.03	31.85	Esférico	0	66.22	15.00	0	Alta
6) Nov-06	2.84	29.08	Esférico	0	61.19	13.19	0	Alta
7) Dic-07	2.62	26.71	Esférico	0	64.6	9.20	0	Alta
8) Dic-08	2.47	24.14	Esférico	0	58.88	13.80	0	Alta
9) Ene-09	2.41	22.32	Esférico	0	52.2	13.20	0	Alta
10) Ene-10	2.27	19.81	Esférico	0	46.8	13.80	0	Alta
11) Feb-11	2.16	17.51	Esférico	0	40.94	12.60	0	Alta
12) Feb-12	2.03	14.51	Esférico	0	31.15	10.80	0	Alta
Plot 2	**Mean**	**Variance**	**Model**	**Nugget**	**Sill**	**Range**	**Nugget/Sill**	**Spatial dependence**
1) Sep-01	2.48	27.47	Esférico	0	80.00	8.99	0	Alta
2) Sep-02	2.37	25.55	Esférico	0	74.62	11.4	0	Alta
3) Oct-03	2.25	23.66	Esférico	0	69.72	9.59	0	Alta
4) Oct-04	2.06	21.01	Esférico	0	61.50	11.21	0	Alta
5) Nov-05	1.93	18.89	Esférico	0	54.40	9.00	0	Alta
6) Nov-06	1.77	16.61	Esférico	0	48.79	11.4	0	Alta
7) Dic-07	1.64	15.17	Esférico	0	44.79	9.00	0	Alta
8) Dic-08	1.54	13.99	Esférico	0	41.60	9.00	0	Alta
9) Ene-09	1.41	12.71	Esférico	0	37.44	9.00	0	Alta
10) Ene-10	1.31	10.95	Esférico	0	32.76	9.59	0	Alta
11) Feb-11	1.98	5.53	Esférico	0	12.90	9.60	0	Alta
12) Feb-12	1.27	4.92	Esférico	0	9.02	12.98	0	Alta
Plot 3	**Mean**	**Variance**	**Model**	**Nugget**	**Sill**	**Range**	**Nugget/Sill**	**Spatial dependence**
1) Sep-01	4.83	33.96	Gaussiano	0	78.3	7.79	0	Alta
2) Sep-02	4.79	30.69	Gaussiano	0	65.25	7.2	0	Alta
3) Oct-03	4.15	24.31	Gaussiano	0	53.07	7.2	0	Alta
4) Oct-04	3.46	19.4	Gaussiano	0	45.23	7.1	0	Alta
5) Nov-05	3.11	15.52	Gaussiano	0	36.48	8.4	0	Alta
6) Nov-06	2.86	12.8	Gaussiano	0	29.92	7.8	0	Alta
7) Dic-07	2.68	10.73	Gaussiano	0	24.36	8.44	0	Alta
8) Dic-08	2.54	9.39	Esférico	0	21.12	12	0	Alta
9) Ene-09	2.42	8.28	Gaussiano	0	12.9	7.8	0	Alta
10) Ene-10	1.98	5.53	Esférico	0	12.9	9.6	0	Alta
11) Feb-11	1.27	3.49	Gaussiano	0	8.53	6	0	Alta
12) Feb-12	1.25	3.37	Exponencial	0	8.09	6.6	0	Alta
Plot 4	**Mean**	**Variance**	**Model**	**Nugget**	**Sill**	**Range**	**Nugget/Sill**	**Spatial dependence**
1) Sep-01	4.01	24.41	Exponencial	0	49.84	10.62	0	Alta
2) Sep-02	3.62	19.33	Esférico	0	38.27	10.62	0	Alta
3) Oct-03	3.5	18.93	Esférico	0	40.48	10.03	0	Alta
4) Oct-04	3.1	15.3	Exponencial	0	31.68	11.8	0	Alta
5) Nov-05	2.66	11.84	Exponencial	0	26.1	11.2	0	Alta
6) Nov-06	1.97	6.46	Esférico	0	15.48	10.02	0	Alta
7) Dic-07	2.14	8.91	Esférico	0	20.01	10.02	0	Alta
8) Dic-08	1.49	4.93	Gaussiano	0	12.04	9.43	0	Alta
9) Ene-09	1.27	4.92	Esférico	0	9.02	12.98	0	Alta
10) Ene-10	1.22	4.07	Esférico	0	7.47	13.57	0	Alta
11) Feb-11	1.19	3.5	Gaussiano	0	6.3	10.61	0	Alta
12) Feb-12	1.16	3.11	Gaussiano	0	5.73	10.03	0	Alta
Plot 5	**Mean**	**Variance**	**Model**	**Nugget**	**Sill**	**Range**	**Nugget/Sill**	**Spatial dependence**
1) Sep-01	2.02	10.41	Esférico	0	15.84	10.2	0	Alta
2) Sep-02	2.01	9.74	Esférico	0	14.94	7.13	0	Alta
3) Oct-03	1.94	8.53	Esférico	0	13.44	7.02	0	Alta
4) Oct-04	1.79	7.39	Esférico	0	11.85	7.48	0	Alta
5) Nov-05	1.76	7.29	Esférico	0	11.2	6.12	0	Alta
6) Nov-06	1.76	7.37	Esférico	0	11.12	8.31	0	Alta
7) Dic-07	1.73	6.88	Esférico	0	11.44	9.12	0	Alta
8) Dic-08	1.57	5.74	Esférico	0	10.08	9.6	0	Alta
9) Ene-09	1.5	5.66	Esférico	0	9.35	10.08	0	Alta
10) Ene-10	1.46	5.18	Esférico	0	8.29	7.92	0	Alta
11) Feb-11	1.44	5.08	Esférico	0	8.16	9.36	0	Alta
12) Feb-12	1.46	5.01	Esférico	0	8.17	9.12	0	Alta
Plot 6	**Mean**	**Variance**	**Model**	**Nugget**	**Sill**	**Range**	**Nugget/Sill**	**Spatial dependence**
1) Sep-01	6.54	51.01	Esférico	0	57.67	10.87	0	Alta
2) Sep-02	6.35	47.92	Esférico	0	53.9	8.31	0	Alta
3) Oct-03	6.17	45.34	Esférico	0	54.4	8.16	0	Alta
4) Oct-04	6.11	44.95	Esférico	0	53.46	7.68	0	Alta
5) Nov-05	5.93	39.81	Esférico	0	47.87	8.16	0	Alta
6) Nov-06	5.56	35.93	Esférico	0	45.9	8.16	0	Alta
7) Dic-07	5.33	33.63	Esférico	0	44.52	8.16	0	Alta
8) Dic-08	5.21	31.17	Esférico	0	42	8.16	0	Alta
9) Ene-09	5.03	29.16	Esférico	0	41.16	8.16	0	Alta
10) Ene-10	5.12	28.56	Esférico	0	40.18	8.15	0	Alta
11) Feb-11	4.99	26.65	Esférico	0	39.01	8.16	0	Alta
12) Feb-12	4.84	25.03	Esférico	0	37.26	8.83	0	Alta

n): número de parcela.

Table 3. Percentage of area infected and not infected by iron spot in coffee plots in the municipality of Amatepec, State of Mexico, from September 2021 to February 2022.

Plot 1	Infected area %	Non-infected área %	Plot 4	Infected area %	Non-infected área %
1) Sep-01	44	56	1) Sep-01	41	59
2) Sep-02	45	55	2) Sep-02	41	59
3) Oct-03	48	52	3) Oct-03	43	57
4) Oct-04	48	52	4) Oct-04	44	56
5) Nov-05	49	51	5) Nov-05	44	56
6) Nov-06	50	50	6) Nov-06	45	55
7) Dic-07	50	50	7) Dic-07	44	56
8) Dic-08	48	52	8) Dic-08	42	58
9) Ene-09	46	54	9) Ene-09	41	59
10) Ene-10	45	55	10) Ene-10	40	60
11) Feb-11	43	57	11) Feb-11	40	60
12) Feb-12	42	58	12) Feb-12	38	62
Plot 2	**Infected area %**	**Non-infected área %**	**Plot 5**	**Infected area %**	**Non-infected área %**
1) Sep-01	50	50	1) Sep-01	56	44
2) Sep-02	51	49	2) Sep-02	58	42
3) Oct-03	52	48	3) Oct-03	59	41
4) Oct-04	53	47	4) Oct-04	59	41
5) Nov-05	53	47	5) Nov-05	60	40
6) Nov-06	53	47	6) Nov-06	60	40
7) Dic-07	51	49	7) Dic-07	58	42
8) Dic-08	50	50	8) Dic-08	58	42
9) Ene-09	49	51	9) Ene-09	56	44
10) Ene-10	49	51	10) Ene-10	55	45
11) Feb-11	48	52	11) Feb-11	55	45
12) Feb-12	46	54	12) Feb-12	53	47
Plot 3	**Infected area %**	**Non-infected área %**	**Plot6**	**Infected area %**	**Non-infected área %**
1) Sep-01	67	33	1) Sep-01	71	29
2) Sep-02	68	32	2) Sep-02	72	28
3) Oct-03	69	31	3) Oct-03	73	27
4) Oct-04	69	31	4) Oct-04	73	27
5) Nov-05	69	31	5) Nov-05	74	26
6) Nov-06	70	30	6) Nov-06	75	25
7) Dic-07	69	31	7) Dic-07	74	26
8) Dic-08	67	33	8) Dic-08	73	27
9) Ene-09	67	33	9) Ene-09	71	29
10) Ene-10	66	34	10) Ene-10	70	30
11) Feb-11	65	35	11) Feb-11	68	32
12) Feb-12	65	35	12) Feb-12	67	33

n): número de parcela

Table 4. Costs associated with flutriafol application in coffee plots in the municipality of Amatepec, State of Mexico.

Plot	Period	Amatepec				
		Cost (MXN ha^{-1})		Savings (MXN ha^{-1})	Quantity of fungicide, with estimate of the area with infected plants (L ha^{-1})	
		Conventional	Estimation of the area with infected plants		Conventional	Estimation of the area with infected plants
1	Sep-Feb	$650	$403	$247	0.5	0.310
2	Sep-Feb	$650	$436	$215	0.5	0.335
3	Sep-Feb	$650	$449	$202	0.5	0.345
4	Sep-Feb	$650	$384	$267	0.5	0.295
5	Sep-Feb	$650	$306	$345	0.5	0.235
6	Sep-Feb	$650	$475	$176	0.5	0.365

Geostatistical analysis. Within spatial statistics, geostatistics is commonly used as a tool for modeling biological phenomena in agriculture (Rossi *et al.*, 1992). The use of these techniques has generated more precise knowledge for managing pests and diseases in different types of crops. Tapia-Rodríguez *et al.* (2020), in their study on the spatial distribution of anthracnose (*Colletotrichum gloeosporioides*), reported an aggregated pattern in all sampling zones. The maps obtained using Ordinary Kriging reveal aggregation centers, enabling targeted control measures against pests and diseases in crops (Esquivel and Jasso, 2014; Moral, 2004; Rivera *et al.*, 2018).

The theoretical semivariograms obtained in this study corresponded to three types (spherical, exponential, and Gaussian). These fitted models demonstrated 98% reliability, indicating that more than 90% of the total variation is attributable to spatial dependence at the sampling scale (Acosta-Guadarrama *et al.*, 2017; Maldonado *et al.*, 2017).

The spherical model indicates that *Mycosphaerella coffeicola* occurs in greater abundance in certain areas of the plot and that aggregation centers are random. This may suggest the presence of previous inoculum sources or the concentration of the pathogen in specific zones due to wind movement. Studies by Ramírez *et al.* (2011) indicate that the fit of the spatial distribution of *Sporisorium reilianum* to the spherical model suggests spatial heterogeneity in disease expression within these areas.

The exponential models obtained indicate that the disease develops along irregular boundaries within the plots, revealing a discontinuous spatial distribution. Similarly, Quiñones-Valdez *et al.* (2018) report that when rust severity fits an exponential model, the disease displays an aggregated spatial distribution but with a distinctive feature: this aggregation develops in an irregular pattern.

The Gaussian model indicates that *Mycosphaerella coffeicola* occurs continuously within the plots, as infection progresses among neighboring plants. Similar results were reported by Sánchez *et al.* (2015) in a study on the spatial pattern of maize head smut, where aggregation centers of the disease were found to be continuous yet compact, implying the pathogen's ability to advance into adjacent plots. A high level of spatial dependence was observed across all plots, consistent with the findings of Tapia-Rodríguez *et al.* (2020) and Sánchez *et al.* (2015).

Estimation of the area with infected plants and its economic impact. The fungus that causes iron spot does not invade 100% of the area; this suggests that certain factors limit the pathogen's dispersal and complete establishment within the plot. Similar behavior has been reported for other fungal pests by Tapia-Rodríguez *et al.* (2020) and Pino-Miranda *et al.* (2022). The findings of this study open the door to targeted application of control measures in areas infected with *M. coffeicola*, making it feasible to achieve economic savings.

CONCLUSIONS

Geostatistics provided a more precise analysis of the spatial behavior of iron spot. Classical methods—such as the Dispersion Index, Green's Index, and Poisson and Negative Binomial distributions—did not yield a conclusive view of the disease's spatial pattern, underscoring the importance of adopting spatial approaches for improved analysis. Through geostatistics, the spatial distribution of iron spot was modeled, revealing aggregation in specific areas. The maps generated using Ordinary Kriging allowed the visualization of disease aggregation centers, enabling the implementation of preventive and targeted control actions.

The detailed spatial modeling revealed that the percentage of total infected area ranged from 38% to 75% across the different sampling periods. This quantification demonstrates the economic impact of precision management: targeted application of fungicides only in infected areas can potentially reduce the use of agricultural inputs. Therefore, the use of geostatistics not only improves epidemiological understanding but also optimizes input use, generating economic benefits and reducing environmental impact.

Acknowledgments

The authors thank the coffee producers of the municipality of Amatepec, State of Mexico, for granting access to their plantations and for the facilities provided during the study. We also acknowledge the Faculty of Agricultural Sciences of the Universidad Autónoma del Estado de Mexico for logistical support and for providing access to the Laboratory of Entomological and Technological Research in Precision Agriculture for the development of this research.

REFERENCES

Acosta-Guadarrama AD, Ramírez-Dávila JF, Rivera-Martínez R, Figueroa-Figueroa DK, Lara Díaz AV, *et al*. 2017. Distribución espacial de *Trips* spp. (Thysanoptera) y evaluación de su control mediante el depredador *Amblyseius swirskii* en el cultivo de aguacate en México. Southwestern Entomologist 42:435–446. https://doi.org/10.3958/059.042.0214

Arce AI, Suzán AH, García RO, Arce AI, Suzán AH, *et al*. 2016. Biotic factors associated with the spatial distribution of the mistletoe *Psittacanthus calyculatus* in a tropical deciduous forest of central Mexico. Botanical Sciences 94(1):89–96. https://doi.org/10.17129/BOTSCI.263

Díaz AVL, Dávila JFR, Zamora FIM, Figueroa DKF, Guadarrama ADA, *et al*. 2018. Simulación espacial de *Claviceps gigantea* (Fuentes, de la Isla, Ullstrup y Rodríguez) en el Estado de México. Revista Mexicana de Ciencias Agrícolas 9(1):95-109. https://doi.org/10.29312/remexca.v9i1.850

Esquivel HV y Jasso GY. 2014. Distribución espacial y mapeo de gusano soldado en seis localidades del Estado de México, en el año 2011. Revista Mexicana de Ciencias Agrícolas 5(6):923-935. https://www.scielo.org.mx/pdf/remexca/v5n6/v5n6a2.pdf

Guzmán OA y Rivillas CA. 2008. Relación de *Glomus manihotis* y *G. fasciculatum* con el crecimiento de plantas de café y la severidad de la mancha de hierro. Cenicafé 58(3):236-257. https://biblioteca.cenicafe.org/bitstream/10778/171/1/arc058%2803%29236-257.pdf

Isaaks E and Srivastava M. 1988. Spatial continuity measures for probabilistic and deterministic geostatistics. Mathematical Geology 20(4):313-341. https://doi.org/10.1007/BF00892982

Jokar M. 2023. Spatial distribution of cotton bollworm in southeastern shores of the Caspian Sea, Golestan Province, Iran. Current Applied Science and Technology 23:10-55003. https://doi.org/10.55003/cast.2022.01.23.014

Leguizamo SG, Rubí AM, Salgado SM y Ramírez DJF. 2023. Panorama de la cafeticultura en el contexto internacional, nacional y en el Estado de México. Pp: 21-45. *In*: Herrera TF, Rubí AM y Rivera RCR (eds.). Café mexiquense Producción, mercado y política pública. IICA. México. 392 p.

Maldonado ZFI, Ramírez DJF, Rubí AM, Antonio NX y Lara DAV. 2017. Distribución espacial de trips en aguacate en Coatepec Harinas, Estado de México. Revista Mexicana de Ciencias Agrícolas 7(4):845-856. https://www.scielo.org.mx/pdf/remexca/v7n4/2007-0934-remexca-7-04-00845-en.pdf

Moral GFJ. 2004. Aplicación de la geoestadística en las ciencias ambientales. Ecosistemas 13(0): 78–86. https://www.revistaecosistemas.net/index.php/ecosistemas/article/view/582.

Pérez CA, Ramírez DJF y Figueroa FDK. 2023. Comportamiento de las poblaciones de roya del café (*Hemileia vastatrix* Berkeley y Broome) en parcelas de Amatepec, Estado de México. Acta Universitaria 33:1-14. https://doi.org/10.15174/au.2023.3870

Pino-Miranda E, Ramírez-Dávila JF, Serrato-Cuevas R, Mejía-Carranza J y Tapia-Rodríguez A. 2022. Spatial and temporal distribution of ojo de gallo (*Mycena citricolor*) in coffee plantations of the State of Mexico. Revista Mexicana de Fitopatología 40(3):433-446. https://doi.org/10.18781/R.MEX.FIT.2204-2

Quiñones-Valdez R, Sánchez-Pale JR, Castañeda-Vildozola Á, Franco-Mora O y Ruíz-Orta A. 2018. Incidencia, severidad y distribución espacial de *Uromyces transversalis* en una nueva región del Estado de México. Scientia Fungorum 48: 87-94. https://www.scielo.org.mx/pdf/sf/v48/2594-1321-sf-48-87.pdf

Ramírez JF, González A, Sánchez PJR y León CD. 2011. Modelización y generación de mapas del comportamiento espacial de *Sporisorium reilianum* ((Kühn) Langdon y Fullerton) en Estado de México, México. Revista de la Facultad de Ciencias Agrarias. Universidad Nacional de Cuyo 43:157-173. https://www.scielo.org.ar/scielo.php?pid=S1853-86652011000200013&script=sci_arttext

Ramírez-Dávila JF y Porcayo-Camargo E. 2008. Distribución espacial de las ninfas de *Jacobiasca lybica* (Hemiptera: Cicadellidae) en un viñedo en Andalucía, España. Revista Colombiana de Entomología 34(2):169-175. https://doi.org/10.25100/socolen.v34i2.9282.

Ramos IZ, Dos santos LA, Rego MD, Tassinari RR, Viana JP, *et al*. 2021. Potencial biocida de extractos de *Jatropha curcas* L. sobre hongos *Hemileia vastatrix* y *Cercospora coffeicola*: agentes causales de dos principales enfermedades del café. Functional Plant Breeding Journal 3 (1):23-32. http://www.fpbjournal.com/fpbj/index.php/fpbj/article/view/103

Rivera-Martínez MR, Ramírez-Dávila JF y Acosta-Guadarrama AD. 2018. Distribución espacial de las poblaciones de huevos de *Bactericera cockerelli* Sulc. en el cultivo de tomate de cáscara (*Physalis ixocarpa* Brot.). Acta Universitaria 28(5): 24-33. https://doi.org/10.15174/au.2018.1944

Rossi RE, Mulla DJ, Journel AG and Franz EH. 1992. Geostatistical tools for modeling and interpreting ecological spatial dependence. Ecological Monographs 62(2):277–314. https://doi.org/10.2307/2937096

Sánchez JR, Ramírez JF, González A y León C. 2015. Patrón espacial del carbón de la espiga del maíz en diferentes localidades del Estado de México. Revista Mexicana de Ciencias Agrícolas 6(7): 1467-1480. https://www.scielo.org.mx/pdf/remexca/v6n7/v6n7a4.pdf

SENASICA. 2016. Mancha de hierro *Mycosphaerella coffeicola* (Cooke) J. A Stevens y Wellman Ficha Técnica No. 46. SENASICA, Servicio Nacional de Sanidad, Inocuidad y Calidad Agroalimentaria. México. 8p.

SIAP. 2025. Servicio de Información Agroalimentaria y Pesquera. http://www.siap.sagarpa.gob.mx (Consulta: marzo 2025).

Tapia-Rodríguez A, Ramírez-Dávila JF, Salgado-Siclán ML, Castañeda-Vildózola Á, Maldonado-Zamora FI, *et al*. 2020. Distribución espacial de antracnosis (*Colletotrichum gloeosporioides* Penz) en aguacate en el Estado de México, México. Revista Argentina de Microbiología 52(1):72–81. https://doi.org/10.1016/j.ram.2019.07.